Experimental study and a short kinetic model for high temperature oxidation of methyl methacrylate

Shanmugasundaram Dakshnamurthy, Denis A. Knyazkov, Artem M. Dmitriev, Oleg P. Korobeinichev, Elna J.K. Nilsson, Alexander A. Konnov, Krithika Narayanaswamy

Supplementary Material

Contents

1 Experimental details

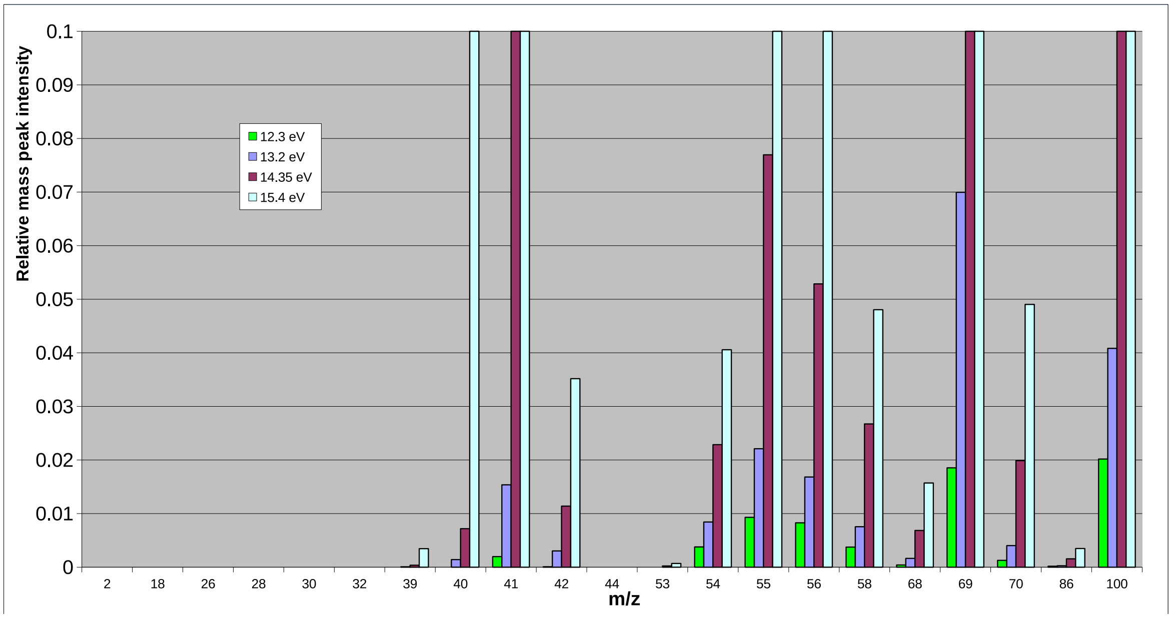

(a)

Figure S1: Relative intensities of selected mass peak for methyl methacrylate/Ar gas mixture at different energies of ionizing electrons (12.3-15.4 eV).

Table S1: Relative intensities of selected mass peaks, which have relevance to this work, for methyl methacrylate/Ar gas mixture at different energies of ionizing electrons (12.3-15.4 eV). Mass peaks, which are not tabulated, had not been measured.

m/z	**12.3 eV**	**13.2 eV**	**14.35 eV**	**15.4 eV**
2	0	0	0	0
18	0	0	0	0
26	0	0	0	0
28	0	0	0	0
30	0	0	0	0
32	0	0	0	0
39	0	7.30507163289619E-05	0.000364925	0.0034551315
40	0	0.0014144443	0.007188215	0.1856791298
41	0.0019730076	0.0153648307	0.165054815	0.5628966322
42	0.000081347	0.0030325767	0.011396899	0.0351760639
44	0	0	0	0
53	0	0	0.0002260622	0.000692059
54	0.0037784337	0.0084328275	0.0228618033	0.0405711064
55	0.009300896	0.0221043912	0.0769441053	0.1611435042
56	0.0082763979	0.0168272808	0.0528640086	0.112402074
58	0.0037472863	0.0075499673	0.0267302065	0.0480398657
68	0.0004069782	0.0016399752	0.0068468141	0.0157129503
69	0.0185327292	0.0699527485	0.3763249153	1
70	0.0012732212	0.0040268618	0.0198882413	0.0490343097
86	0.0001795493	0.0002713766	0.0015626282	0.0034829807
100	0.0201775732	0.0408334938	0.1336613796	0.2709813892

Table S2: Variation of burning velocities of MMA for various unburnt temperatures and equivalence ratio at 1 atm. The uncertainty of all burning velocities in the tabulated experimental data is ±1 cm/s.

	Burning velocities in cm/s			
T (K) / ϕ	**298**	**318**	**338**	**358**
0.7	21.04	24.37	27.63	31.77
0.8	29.25	32.81	36.88	41.63
0.9	35.48	39.55	44.07	49.40
1.0	39.63	44.07	48.81	54.11
1.1	41.33	45.77	50.74	55.82
1.2	40.14	44.59	49.33	54.52
1.3	36.6	40.22	45.03	49.93

2 Comparison of detailed and reduced model

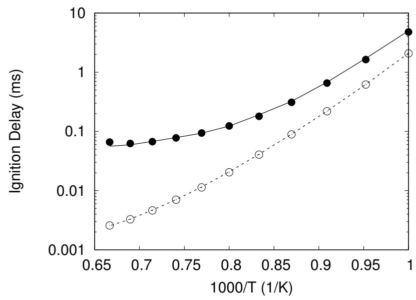

(a) $\phi = 0.5$

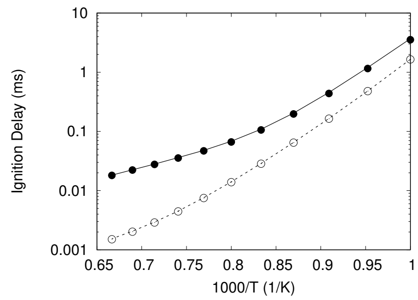

(b) $\phi = 1$

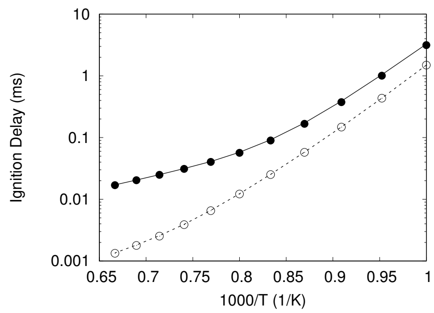

(c) $\phi = 1.5$

Figure S2: Ignition delays in a constant volume reactor at $P = 1, 20\,\mathrm{atm}$; lines - detailed mechanism (solid: 1 atm, dashed: 20 atm), symbols - skeletal mechanism.

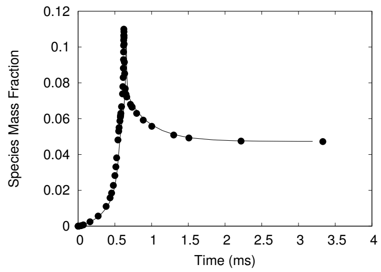

(a) CO

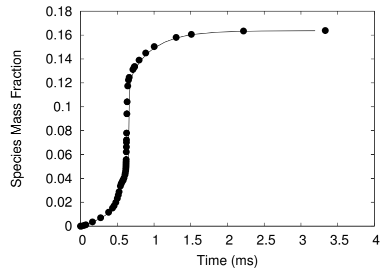

(b) CO_2

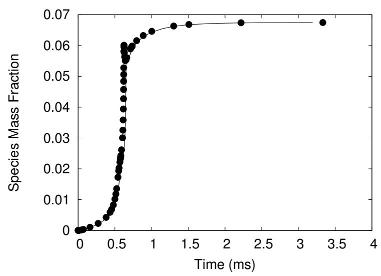

(c) H_2O

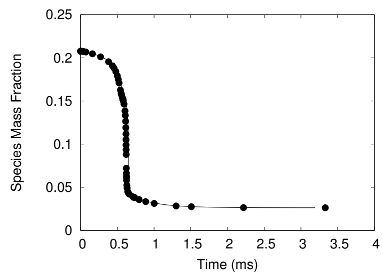

(d) O_2

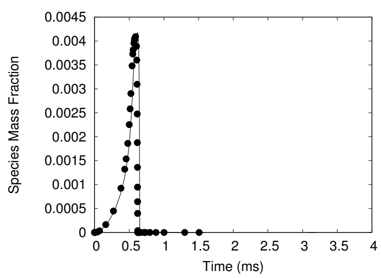

(e) CH_4

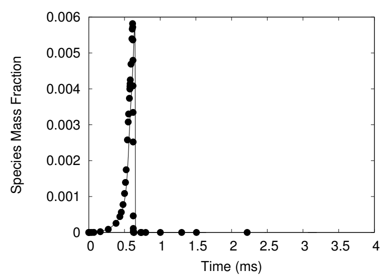

(f) C_2H_2

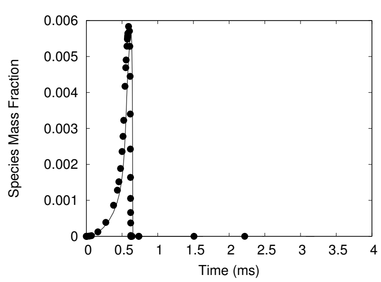

(g) C_2H_4

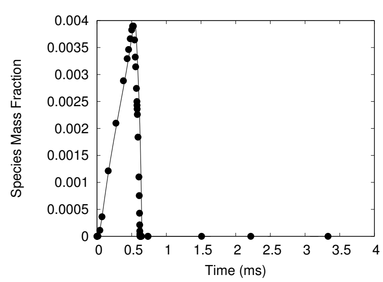

(h) C_2H_6

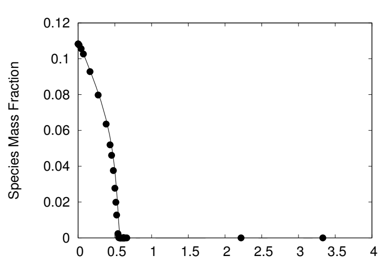

(i) Methylmethacrylate

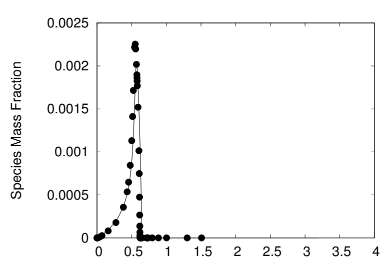

(j) C_3H_6

Figure S3: Species profiles in a flow reactor at $\phi = 1.0$, $P = 1\,\mathrm{atm}$, initial temperature $T = 1100\,\mathrm{K}$, lines - detailed mechanism, symbols - skeletal mechanism.

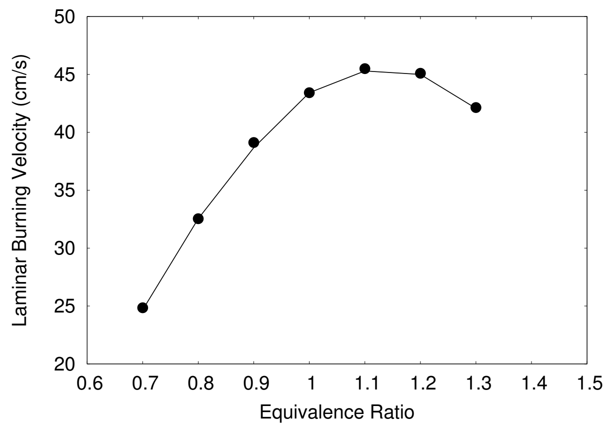

(a) Burning Velocity of MMA

Figure S4: Laminar burning velocities of MMA at an unburnt temperature T_u = 298 K; lines - detailed mechanism , symbols - skeletal mechanism (at 1 atm pressure)

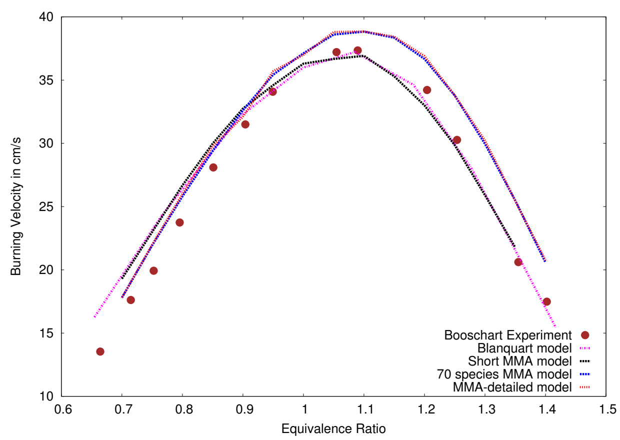

(a) Laminar burning velocity of CH_4

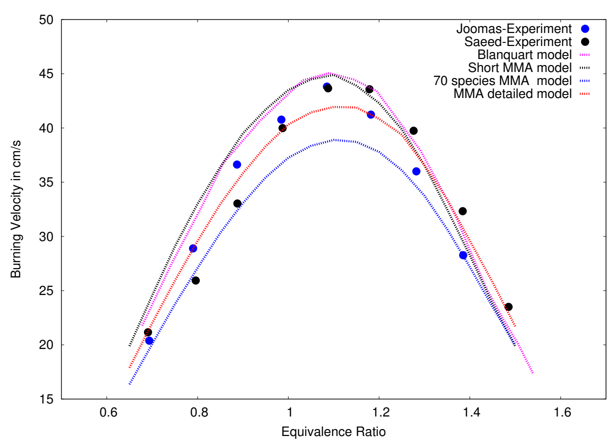

(b) Laminar burning velocity of C_3H_6

Figure S5: Laminar burning velocities of methane and propene at an unburnt temperature T_u = 298 K; lines - simulation, red(line)- Blanquart [1] ; symbols - experiments (at 1 atm pressure), brown (symbol)- Booschart [2], blue (symbol)- Joomas [3], black (symbol)- Saeed [4].

3 Main oxidation pathways of MMA

At high temperatures, MMA is consumed via H-abstraction by the attack of H, OH and O radicals at the allylic, alkylic and vinylic sites, addition of O and OH radicals at C=C of MMA, and unimolecular decomposition. The fuel radicals $CH_2 = C(CH_{\mathbf{2}}) - C(= O) - O - CH_3$ (radical at allyl site), $C\mathbf{H} = C(CH_3) - C(= O) - O - CH_3$ (radical at vinyl site) and $CH_2 = C(CH_3) - C(= O) - O - CH_{\mathbf{2}}$ (radical at alkyl site), formed via the H-abstraction reactions further undergo β-scission to form allene, propyne, I-C_3H_5CO and their corresponding products, respectively. The addition of O and OH radicals at an internal carbon site (across C=C) produces $CH_3 - C(= O) - CH_2^*$ and $CH_3 - C(= O) - CH_3$ (acetone), respectively, along with CH_3OCO. The species CH_3OCO is also produced via OH addition at terminal carbon through the formation of intermediate radicals, MP2J and MP3J. Unimolecular decomposition of MMA also yields CH_3OCO radicals via breaking of C–C(=O) bond, while produces I-C_3H_5CO and methoxy (CH_3O) radicals via scission of C(=O)–OCH_3 bond.

The radical, CH_3OCO, formed from the aforementioned pathways decomposes via two routes to give (i) methoxy radical and carbon monoxide and (ii) methyl radical and carbon dioxide.

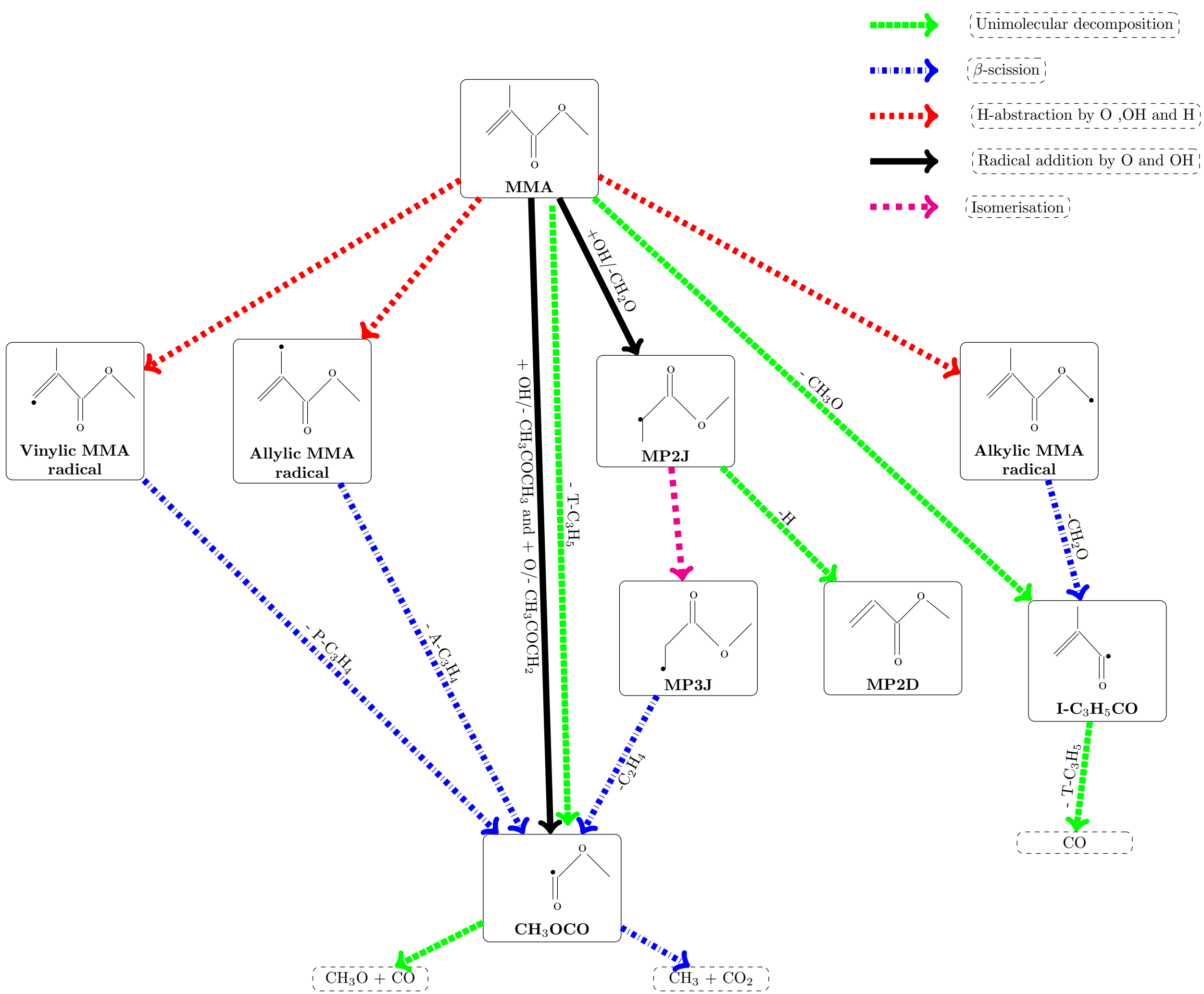

Figure S6: Schematic layout of the main pathways in the derived skeletal model for methylmethacrylate oxidation.

4 Comparison of short MMA model with the detailed model for sub-atmospheric pressure flat flames

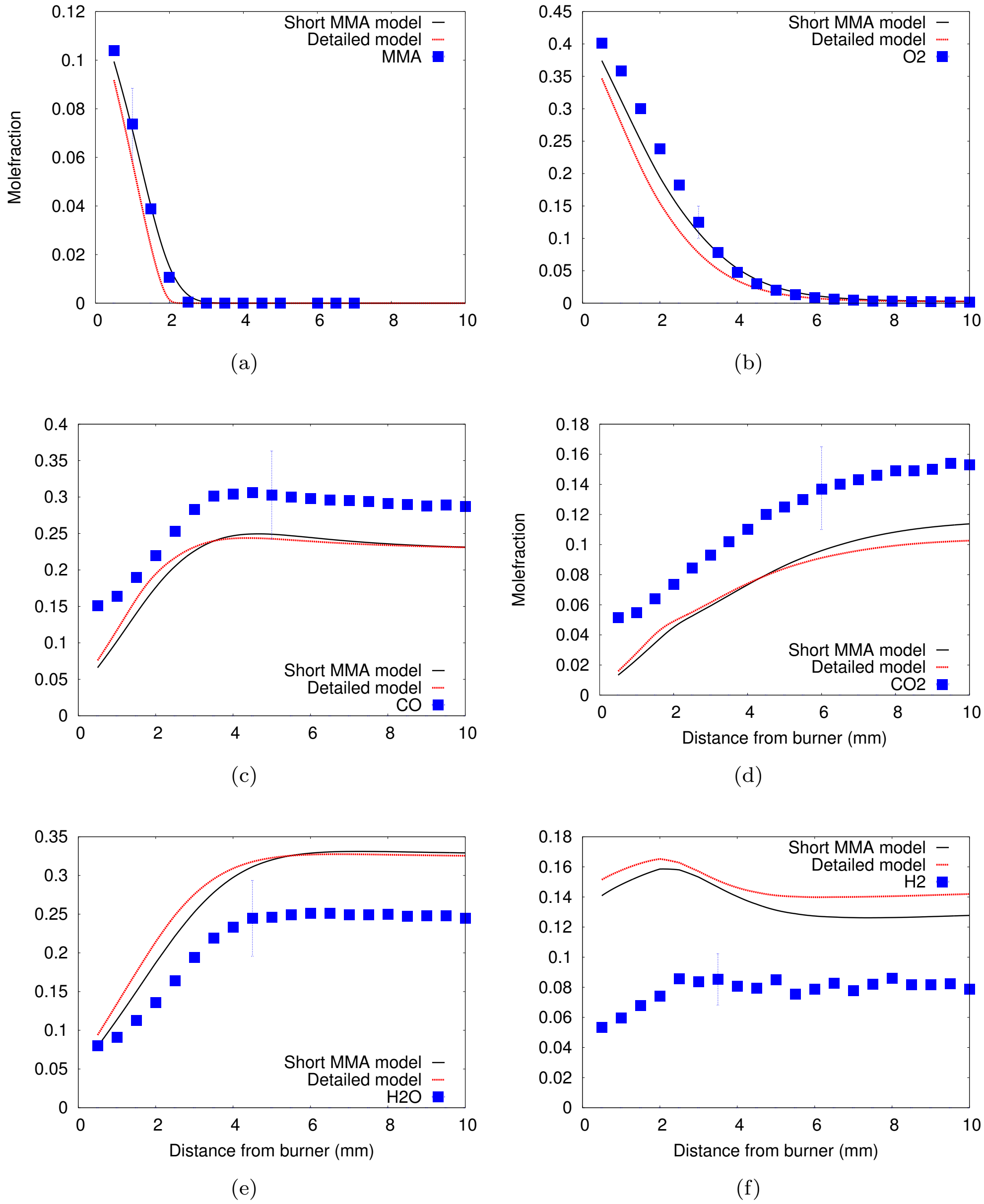

Figure S7: Comparison of short MMA model with the detailed model for major species profiles of Laminar flat flame at sub-atmospheric condition ; symbols-experiment, lines-simulation.

The experimental major species profiles are not predicted within the experimental uncertainty range by the short MMA model or the original detailed model, while the corresponding simulations for the atmospheric-pressure flame show a good agreement (Fig. 4 in the main article). Flux analysis performed in the low pressure flame case suggests that the reactions producing/consuming the major species are similar to those of the atmospheric flames, and there are no pressure-dependent reactions in this list, whose pressure dependence is not accounted for. Nonetheless, since the present work focuses on flames at atmospheric pressures for fire research applications, resolving this discrepancy is reserved for a future study when the application demands the validity of the model at lower pressures.

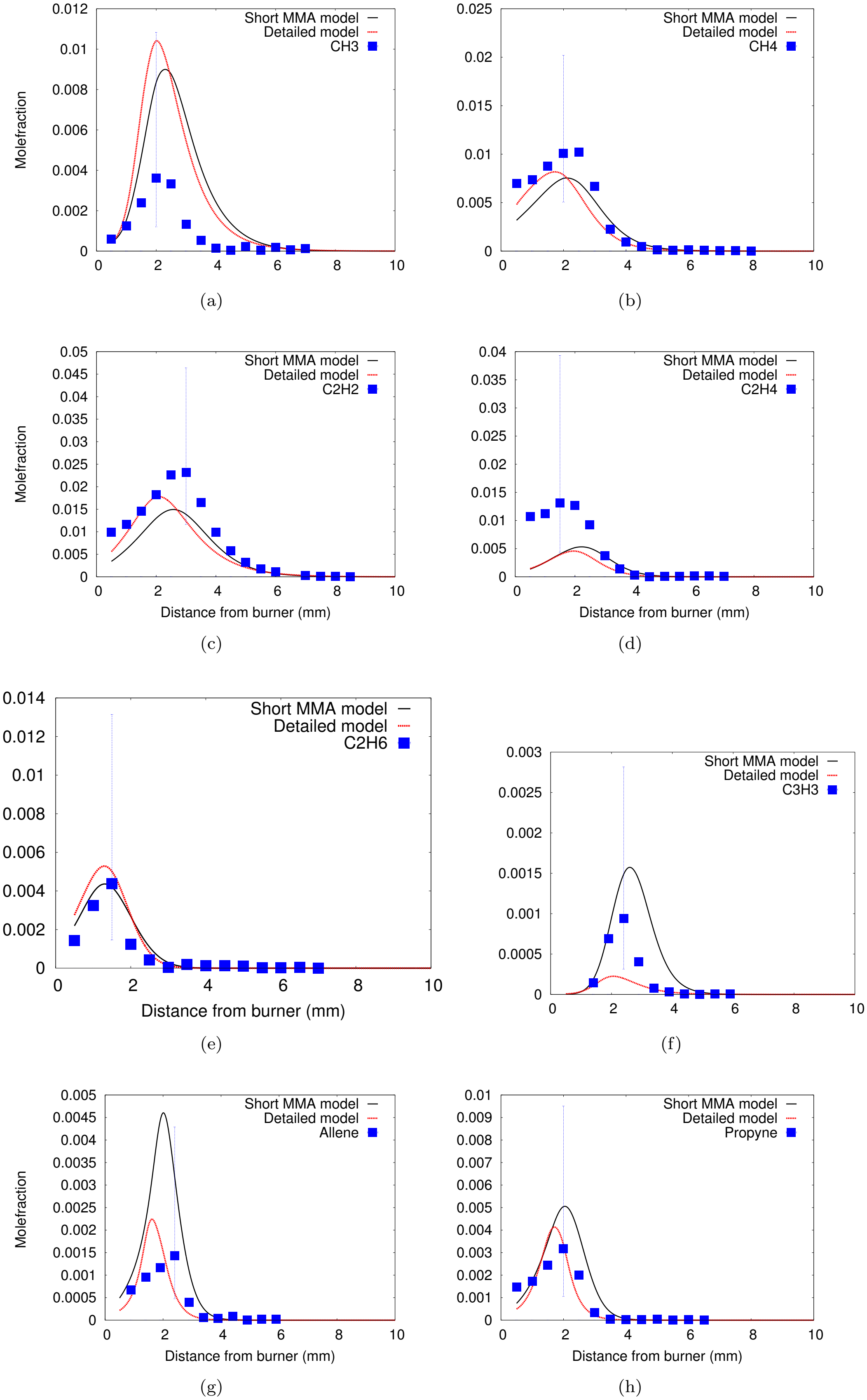

Figure S8: Comparison of of short MMA model with the detailed model for C_1, C_2 and C_3 species profiles of laminar flat flame at sub-atmospheric condition; symbols-experiment, lines-simulation.

5 Comparison of short MMA model with the detailed model for atmospheric pressure flat flames

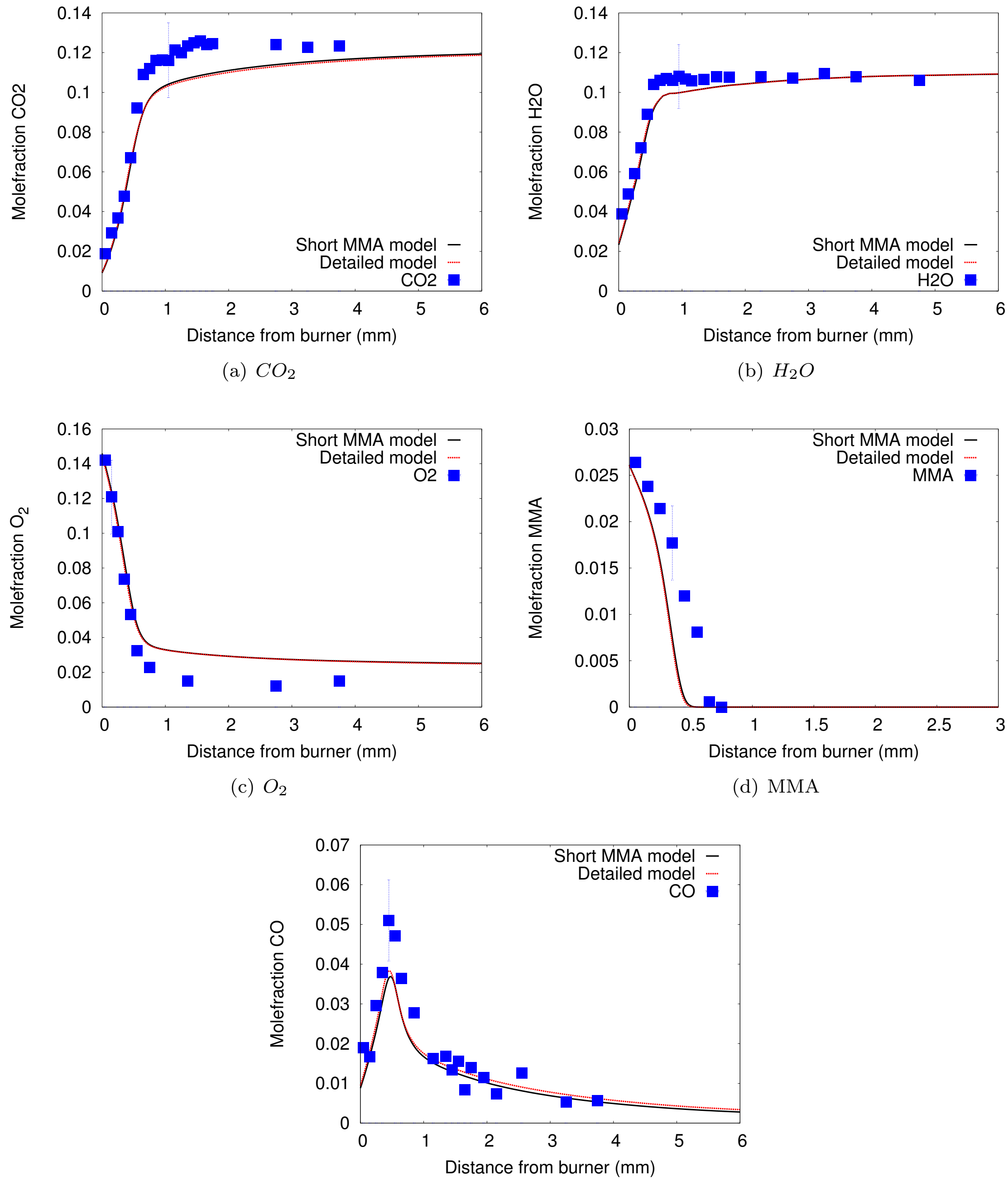

(a) CO_2

(b) H_2O

(c) O_2

(d) MMA

(e) CO

Figure S9: Comparison of short MMA model with the detailed model for major species profiles of laminar flat flame at atmospheric condition ; symbols-experiment, lines-simulation.

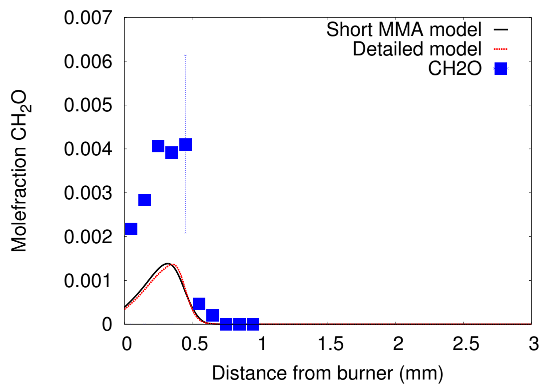

(a) CH_2O

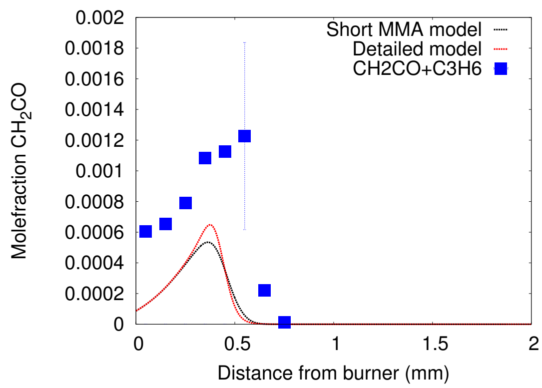

(b) $CH_2CO + C_3H_6$

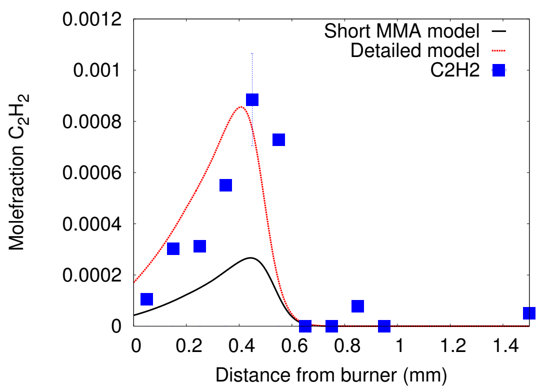

(c) C_2H_2

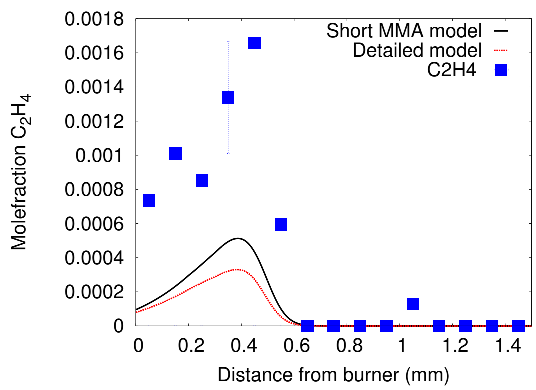

(d) C_2H_4

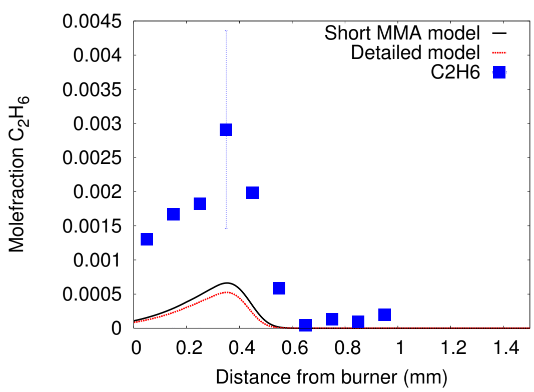

(e) C_2H_6

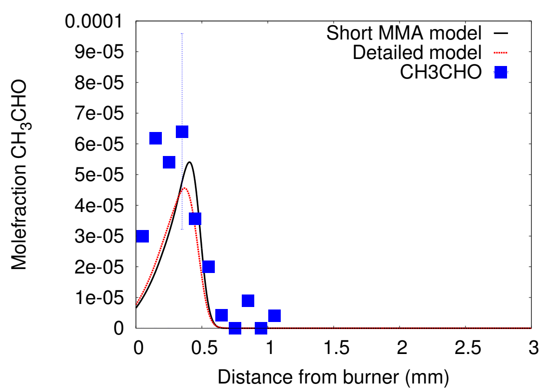

(f) CH_3CHO

Figure S10: Comparison of of short MMA model with the detailed model for C_1 and C_2 species profiles of laminar flat flame at atmospheric condition; symbols-experiment, lines-simulation.

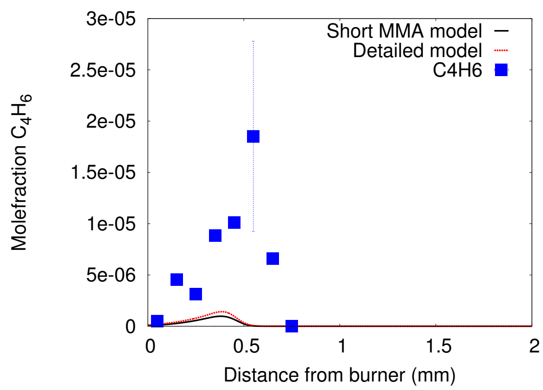

(a) C_4H_6

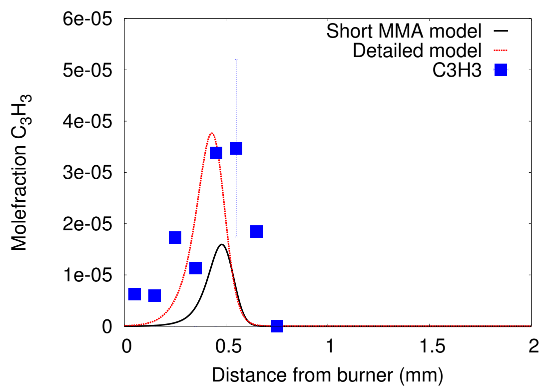

(b) C_3H_3

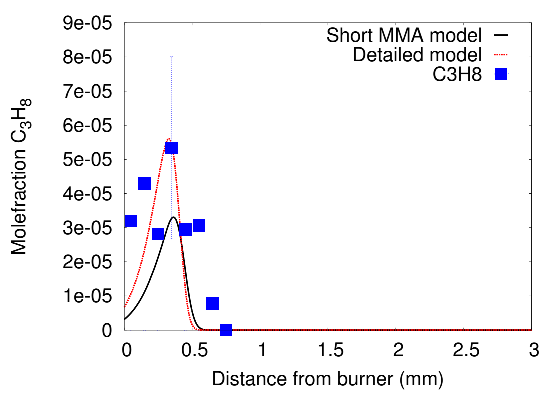

(c) C_3H_8

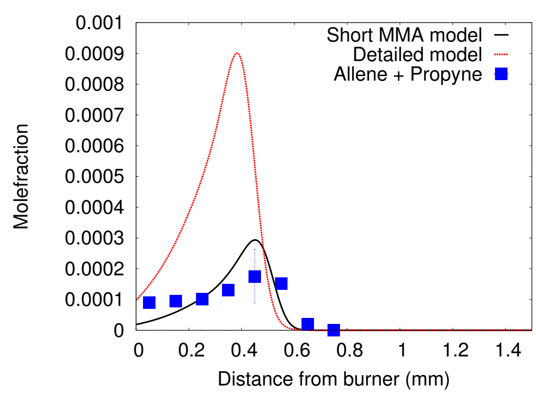

(d) $Allene$

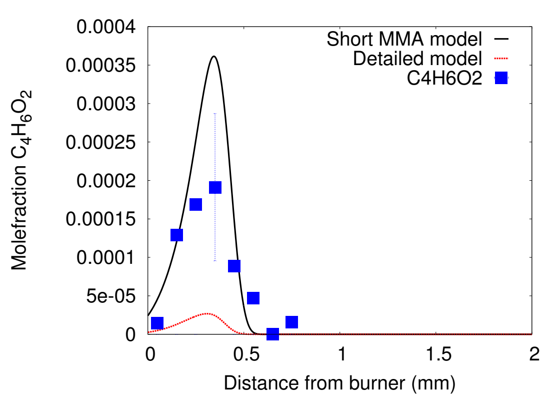

(e) $C_4H_6O_2$

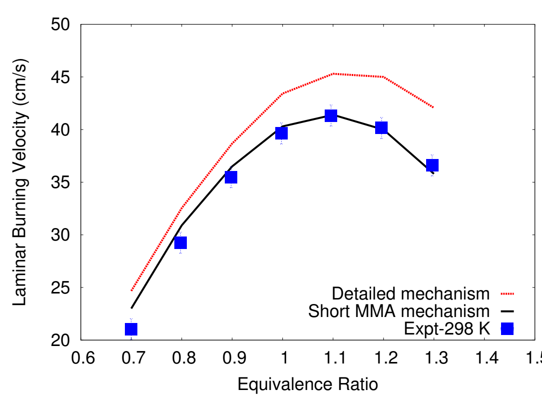

(f) $\mathrm{MMA-Burningvelocites}$

Figure S11: Comparison of short MMA model with the detailed model for C_3, and C_4 species profiles of laminar flat flame and burning velocities of MMA at atmospheric condition; symbols-experiment, lines-simulation.

References

[1] G Blanquart, P Pepiot-Desjardins, and H Pitsch. Chemical mechanism for high temperature combustion of engine relevant fuels with emphasis on soot precursors. *Combustion and Flame*, 156(3):588–607, 2009.

[2] KJ Bosschaart and LPH De Goey. The laminar burning velocity of flames propagating in mixtures of hydrocarbons and air measured with the heat flux method. *Combustion and Flame*, 136(3):261–269, 2004.

[3] Grunde Jomaas, XL Zheng, DL Zhu, and CK Law. Experimental determination of counterflow ignition temperatures and laminar flame speeds of c2–c3 hydrocarbons at atmospheric and elevated pressures. *Proceedings of the Combustion Institute*, 30(1):193–200, 2005.

[4] Khizer Saeed and R Stone. Laminar burning velocities of propene–air mixtures at elevated temperatures and pressures. *Journal of the Energy Institute*, 80(2):73–82, 2007.